Chapter 9

The high latitude seas and Arctic Ocean

Johnny A. Johannessen[1] and Ole B. Andersen[2]

(1) NERSC, Norway
(2) DTU, Denmark

Contents

9.1 Introduction.

Changes in the dynamic topography and ocean circulation between the North Atlantic and the Arctic Ocean result from variations in the atmospheric forcing field and convective overturning combined with changes in freshwater runoff and their pathways, mean sea level, sea ice deformation and water mass transformation. The ocean circulation in this region has been subject to investigations since Helland-Hansen and Nansen (1909). In general, it can be characterized by four regional circulation regimes and cross-regional exchanges and volume transports, namely the Northeast Atlantic, the Labrador Sea and Canadian archipelago, the Nordic and Barents Seas and the Arctic Ocean, as illustrated in Fig. 9.1.

Accurate knowledge of the ocean transport variability together with understanding of the water mass transformations within and across these regions is highly needed to quantify changes in the overturning circulation with acceptable uncertainty. The Atlantic meridional overturning circulation is, among other factors, influenced by: - variations in the upper ocean and sea ice interaction; - ice sheet mass changes and their effect on the regional sea-level change; - changes in freshwater fluxes and pathways; and - variability in the large-scale atmospheric pressure field. For instance, changes in the pathways of the freshwater from the Eurasian runoff forced by shifts in the Arctic Oscillation can lead to increased trapping of freshwater in the Arctic Ocean as presented by Morison et al. (2012) that, in turn, may alter the thermohaline circulation in the sub-Arctic Seas.

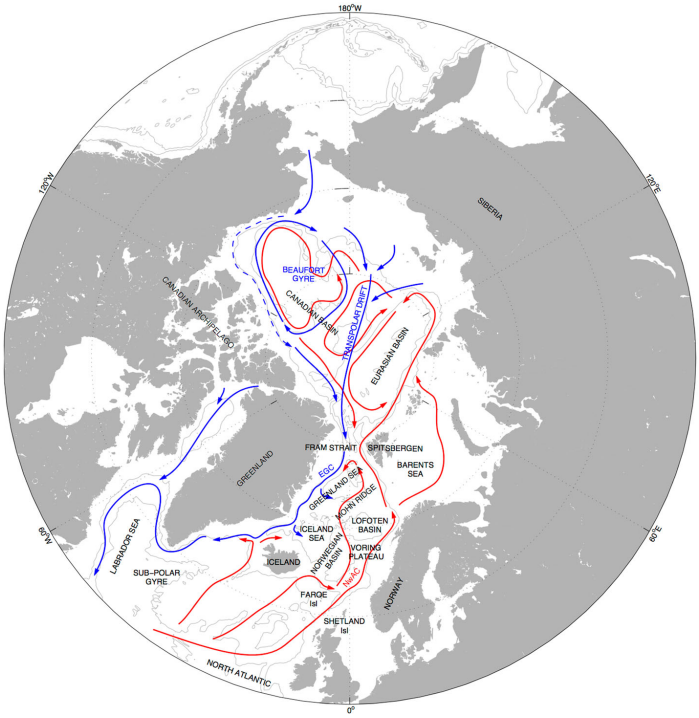

Figure 9.1. *General circulation in the upper ocean of the Arctic Ocean, Nordic Seas, and North Atlantic from Furevik and Nilsen (2005). Red arrows represent the warmer Atlantic Waters, which reside in the surface in the Nordic Seas and submerged in the Arctic Ocean. Blue arrows represent Polar Water, residing in the surface. Bottom contours marked by the 1000 and 3000 m are outlining the shelves and basins.*

The Arctic Ocean is the smallest and shallowest of the world's five major oceans. It covers roughly 4.2%vof the world's ocean and as the average depth of the Arctic Ocean is just 1300 meters it holds only about 1.2% of the total volume of ocean water. The International Hydrographic Organization (IHO) recognizes the Arctic Ocean as an ocean, although some oceanographers call it the Arctic Mediterranean with limited pathways and water exchange with the larger sub-Arctic oceans. The four major pathways include: the Fram Strait between Greenland and Svalbard; the Bearing Strait between Russia and USA; the Canadian Archipelago region and Nares Strait; and the northeastern Barents Sea.

Besides these open boundaries the Arctic Ocean has significant input of freshwater from rivers and melting ice-caps Eight of the nine largest rivers contributing freshwater to the Arctic Ocean are located in the Russian sector with the Siberian rivers; Yenisei, Ob, and Lena each providing up to 600 km3 of water per year whereas the Canadian-sector Mackenzie River provides of the order of 340 km3 per year (Aagaard and Carmack, 1989). In addition the melting of the Greenland Ice Sheet and glaciers adds between 200 to 400 km3 freshwater per year (Khan et al. 2015).

The Arctic Ocean currently stores around 84,000 km^3 of freshwater in its surface layer (*Serreze et al*., 2006) and this number seems to be increasing. Measurements from ships and moorings have shown that the deep Arctic basins, in particular the Canada Basin, accumulated up to 10,000 km3 of freshwater during the 1990s and 2000s (Proshutinsky et al., 2009; Krishfield et al., 2014; Rabe et al., 2014). This was confirmed from satellite altimetry by *Giles et al*. (**2012**) who demonstrated that the Beaufort Gyre accumulated 800 ± 200 km^3 of freshwater per year during the 2000's. The freshwater storage in the Arctic Ocean is highly important to monitor, as the enhancement of the freshwater outflow, mainly occurring through the Fram - and Nares Straits, may be able to disrupt the North Atlantic Meridional Overturning Circulation (*Manabe and Stouffer*, **1995**). Such enhanced freshwater outflow has previously been linked to the North Atlantic "Great Salinity Anomalies" of the 1970s, 1980s, and 1990s (*Dickson et al*., **1988**; *Belkin*, **2004**). The "Great Salinity Anomaly" of the 1970s consisted of only ~2000 km^3 excess liquid and solid freshwater export to the North Atlantic

(*Häkkinen*, **1993**). Hence, monitoring the balance and/or sea level budget of the Arctic Ocean freshwater fluxes is climatically important.

There is a growing concern regarding the Arctic region responds to climate change. There is evidence that the Polar Ocean is undergoing rapid climate change resulting from processes including a reduction of sea ice extent, thickness and volume (e.g., *IPCC*, 2013; Kwok et al., 2009; *Stroeve et al*., 2012; Kern et al., 2015, Tilling, 2016). Sea level observations in the Arctic Ocean has traditionally been based on tide gauges. However, the coverage is inhomogeneous and in some regions sparse in time and space. A reasonable amount of tide gauge data (more than 100) is available along the Norwegian and Russian coasts since 195[illegible]. Unfortunately a substantial part of the Russian gauges were discontinued with the collapse of the Soviet Union in the early 1990's. A challenge with many of the Arctic tide gauges is also their location in vicinity of river-mouths and even inside rivers. For instance, the tide gauge Antipaiuta (69°N, 76°E) in the PSMSL database (Holgate, 2013) is located inside the Ob River eustaria nearly 900 km from the open Arctic Ocean.
Consequently a very careful editing of the tide gauges is required to isolate the sea level signals which are of oceanographic origin (Proshutinsky, Volkov, Henry et al, 2012; Svendsen et al., 2014, 2016). Figure 9.2 shows the carefully edited 66 tide gauges by Henry et al., 2012.

9.1.1 Satellite Altimetry in the high latitude and Arctic Ocean

Sea surface height (SSH) is an essential climate variable and global indicator (*IPCC*, 2013) and satellite altimetry is a key component to retrieve this variable. Despite the fact that satellite altimetry is a mature and precise technique for global mean sea level (MSL) monitoring it suffers from increasing uncertainties in the Arctic Ocean region due to a number of factors such as:

- The inclination of the CNES/NASA TOPEX/Poseidon and Jason satellites limits their coverage to 66° N, which means that these satellites does not cover the Arctic Ocean with regular routine sea level observations.
- The European Space Agency satellites ERS-1, ERS-2 and Envisat provided continuous altimetry observations up to nearly 82˚ from 1991 to 2012. Covering 78 % of the Arctic Ocean, they have therefore been fundamental in deriving the long altimeter-based SSH record for the Arctic Ocean (Prandi et al., 2012).
- Standard processing of satellite radar altimetry are faced with severe difficulties in the presence of sea ice and as such they do not provide regular routine monitoring of the Arctic sea level. Sea ice affects the returned radar echo or waveform recorded by the satellite or even prevents it from reflecting off the sea surface. The waveform can become highly complex with multiple peaks resulting from scattering within the sea ice covered footprint. The waveform can also be very specular if returned by water within leads. In any case, the waveform does not resemble a normal open ocean Brown waveform for conventional altimeters and is subsequently often discarded by the Space Agency processing schemes. Moreover, the sea ice contaminates the radiometer observations and hence the ability to provide accurate range corrections. Finally several range corrections are missing and/or are less accurate in the Arctic Ocean. For instance, the tides are less accurate in the Arctic Ocean than elsewhere (Stammer et al., 2014).
- In the northern part of the Nordic Seas and in the Barents Sea nearly 100 % of conventional altimetric data is available for the 1991-2010 period. However this number rapidly decreases when moving into the interior of the Arctic Ocean where an average of only between 5 and 10 % is available (Figure 9.2) during the 1993-2010 period

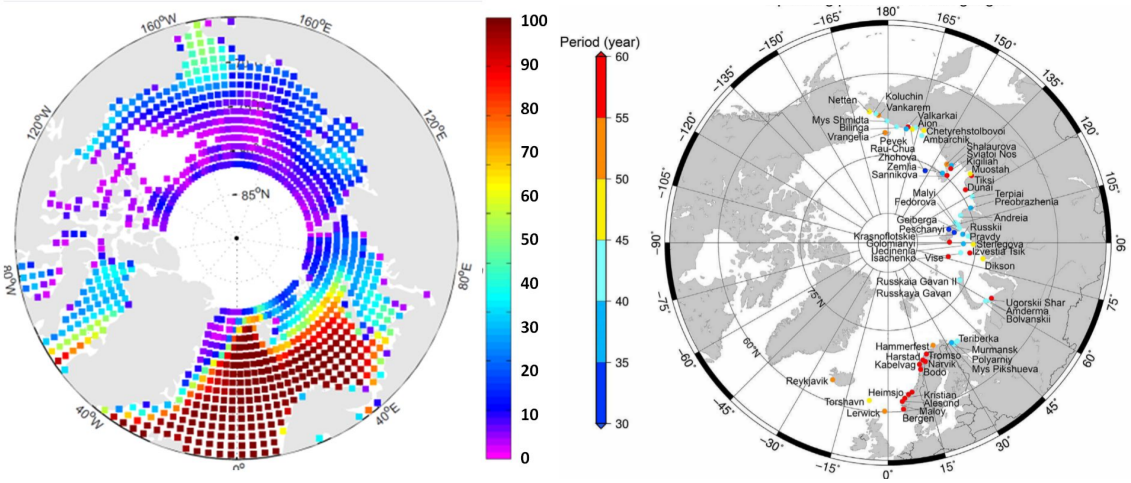

***Figure 9.2**. (left) Percentage of available data along the ERS-1/ERS-2/ENVISAT reference tracks in the RADS standard edited dataset SLA during the 1993-2010 period (from Cheng and Andersen, 2014). (right) Locations of the 66 tide gauge stations selected for the sea level study by Henry et al., (2012).*

In order to increase the coverage and quality of SSH observations in ice affected regions, several new altimeter satellite missions have been launched and operated in the last 15 years such as ICESat, CryoSat-2, Sentinel-3A and SARAL/AltiKa. ICESat provided 17 monthly epochs of laser altimetry up to 86°N between 2003 and 2009 and will likely be continued by ICESat-2 in 2018. The higher resolution (footprint: 50–70 m) and precision of the lidar (shot-to-shot repeatability of ~2–3 cm) onboard ICESat (*Zwally et al.*, 2002) allowed unambiguous identification of open water between ice-floes and therefore importantly supplied a new source of SSH observations in the Arctic Ocean (*Kwok et al.*, 2004).

The CryoSat-2 mission (*Wingham et al.*, 2006), a new generation Earth Explorer mission, acquires the SSH by the single frequency (Ku) Synthetic Aperture Radar (SAR) Interferometric Radar ALtimeter (SIRAL). With an inclination of 92° the altimeter covers 95% of the Arctic Ocean while operating in three different modes. These are conventional or low resolution mode (LRM); the Synthetic Aperture Radar (SAR) mode in which a delay Doppler modulation partitions the radar footprint into a number of along-track slices; and finally the interferometric Synthetic Aperture Radar Mode (SAR-in) in which two receiving antenna chains onboard Cryosat-2 are enabling the detection of the cross-track angle to the prime scatter in the footprint. This SAR-in mode has proven to be particularly useful in the Arctic Ocean (Laxon et al., 2013) as well as for coastal regions (i.e., Abulaitijiang and Andersen, 2015) where the satellite can detect coastal sea level even when the satellite is flying over land close to the coast.

Whereas conventional or LRM observations has a footprint of roughly 100 km2, the SAR and SAR-in modes have a footprint of roughly 4 km2 which means that far fewer observations are affected in the presence of sea ice. This enables the instrument to track sea level in leads and polynyas in the ice covered regions. The delay Doppler modulation of the altimeter signal create a synthesized footprint which is nominally 0.31 km by 1.67 km in the along- and across- track directions (Martin-Puig et al., 2013). Similarly multiple-looks of returns from the surface are used to reduce the noise due to radar speckle (*Bouzinac*, 2013). Cryosat-2 operates in all 3 modes over the Arctic Ocean following a sophisticated mask which changes with time and sea ice coverage. The detection of sea level within leads and polynyas from Cryosat-2 still requires careful examination of the full waveforms (so-called Level-1B data).

In 2013 the French-Indian **S**atellite with **AR**gos and **AL**tiKa (SARAL) was launched in the same orbit as ENVISAT to continue the altimetric record and to test a new Ka-band altimeter with a spatial resolution of 2 km. The ALTIKA instrument measures the ocean surface topography with an accuracy of 8 mm, in comparison to about 2.5 cm for conventional altimeters.

The Sentinel-3A satellite that was successfully launched in 2016 carries a dual frequency (Ku- and C-band) SRAL instrument. SRAL is similar to the SIRAL onboard Cryosat-2, but does not provide the interferometric capabilities as for Cryosat-2. On the other hand it has a microwave radiometer for atmospheric corrections. This satellite is the first-ever satellite to operate in high resolution SAR mode everywhere including the Arctic Ocean up to 81°N. Altogether the continuity of altimetry satellites in principle provides a data record for the Arctic Ocean which by 2016 reaches 25 years.

Returning to the conventional altimeter satellites ERS-1/ERS-2 and ENVISAT, there are basically two approaches to increase the number of reliable SSH observations in the Arctic Ocean. One is the use of a more robust radar waveform retracker tailored to the conditions in the Arctic Ocean; the other is a re-evaluation of existing datasets consisting of fine-tuning/tailoring the editing and re-processing of the data within the Arctic Ocean. The drawback of using robust retrackers (Gommenginger et al., 2011) is that they do not provide estimates of significant wave height.

Retracking of the ERS-2 data was applied by Peacock and Laxon (2004) who developed a robust empirical retracker to extract the sea surface height (SSH) for the 1995-2004 period. More recently Armitage et al., (2016) retracked the ENVISAT data using the same method developed for ERS-2 and recently the combined reprocessed ERS-1 and ERS-2 REAPER dataset have been made available. Wihin the ESA climate change initiative, the SL-CCI has issued the study of a more sophisticated retracking system of ENVISAT in which the data are first classified by ocean surface type in order to separate frozen ocean areas from open water corresponding to leads and polynyas and subsequently using new retracking algorithm for each class. Cheng and Andersen (2013) created an Arctic SSH dataset without retracking but with reprocessing the data by a combination of fine tuning editing criterias for the Arctic Ocean and replacing range and geophysical corrections. Thereby, they retrieved between four and ten times as many SLA observations in large part of the interior of the Arctic Ocean without degrading the quality of the data. In turn, they could derive a time-series of Arctic Ocean SSH anomalies for 20 years. This has recently been updated to a 25-year time-series called DTU-SSH (Andersen and Piccioni, 2016) taking into account 5 additional years of retracked Cryosat-2 SAR altimetry data.

9.2 Mapping the sea ice thickness in the Arctic Ocean

The key approach to derive sea ice thickness estimation in the Arctic Ocean is by satellite altimetry. The caveat is that the uncertainty estimation is challenging and that the existence of in-situ observations of snow depth, snow density and sea ice thickness are sparse. The first comprehensive estimate of changes in sea ice thickness from altimetry was published by Laxon et al. (2003). Exploring radar altimeter measurements from ERS-1/2 and Envisat from the 1990s, they found a strong inter-annual variability in sea ice thickness, and circumpolar thinning of Arctic sea ice. Moreover, Kwok et al. (2009) found a decline in Arctic sea ice thickness of 0.18 m/yr between 2003 and 2008 based on analyses of laser altimeter measurements from NASA's ICESat. At the end of the ICESat period in 2008, a winter thickness of 1.89 m was reported, being 1.75 m lower than the mean sea ice thickness from the 80's based on reported submarine data in the central Arctic (Kwok and Untersteiner, 2011). In comparison, Hendricks et al. (2013) derived a mean sea ice thickness of 1.87 m in the central Arctic in winter of 2012-2013 (October - March) using CryoSat-2 data.

The freeboard, the part of the ice above the water level is obtained by using the elevation over leads as the instantaneous sea surface height and then calculating the difference between the sea surface height and ice floes (Zwally et al., 2002; Kwok et al., 2007; Hendricks et al., 2013). The elevation measurements from leads and ice floes are distinguished by the shape of the waveform based on the pulse peakiness structure (see Figure 9.3). Specular echoes occur when the radar burst is reflected from a smooth, mirror-like surface such as a lead or very thin ice. In these cases the power in the range window rises and falls again very rapidly, creating an echo that looks like a spike (Figure 9.3, right). Diffuse echoes occur when the radar burst is reflected from a rougher surface such as an ice floe. In these cases the power in the range window rises rapidly but gently decays, creating an echo that looks like a step (Figure 9.3, left). After retracking the range and applying necessary corrections (e.g. Doppler range, the ionospheric, the dry tropospheric and the modelled wet tropospheric, ocean tide,

long-period tide, loading tide, earth tide, pole tide and inverse barometer corrections), and filters (removal of complex waveforms, failed re-tracking and echoes that yielded elevations more than 2 m from the mean dynamic sea surface height) the local sea level at ice floe locations is interpolated from nearby lead elevations. The freeboard is then calculated as the difference of radar altimetry measured ice floe elevation and the local sea level. As the freeboard measurement is known to be noisy, it is necessary to average several measurements. While the radar altimeter signal is assumed to be reflected from the snow and ice interface (Beaven et al., 1995), thus providing the ice freeboard, the laser signal is reflected from the air-snow interface, and hence provides the snow plus the ice freeboard. Assuming hydrostatic equilibrium, the freeboard can be converted into an estimate of sea ice thickness based on given knowledge of the sea ice density as well as the snow depth and snow density.

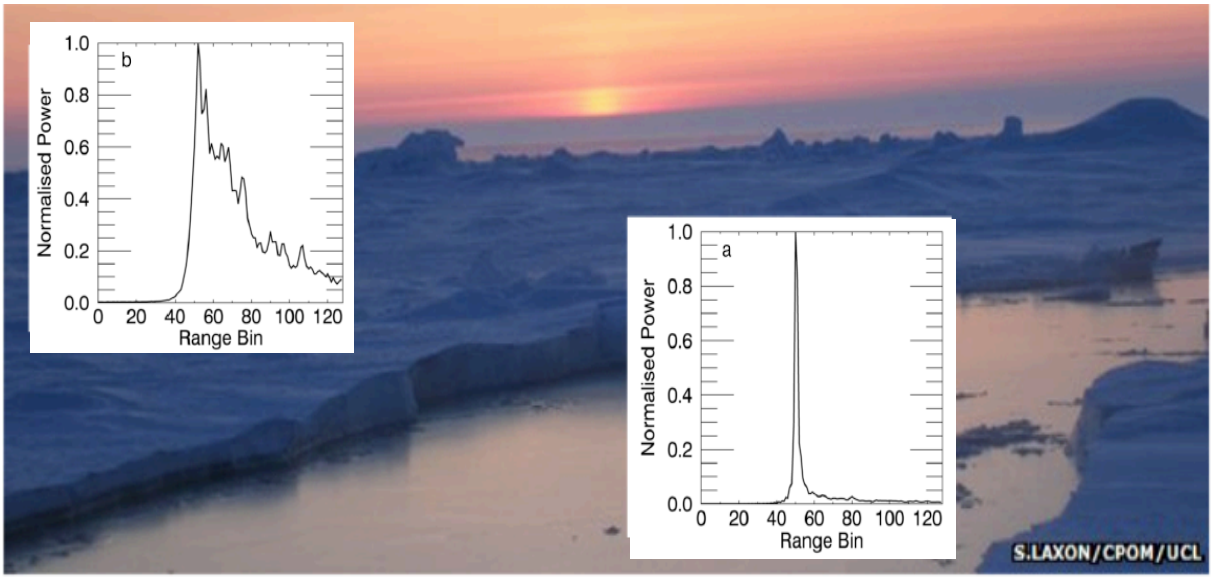

Figure 9.3 *Typical radar altimeter waveforms representing sea ice (left) and leads (right). Courtesy S. Laxon, UCL.*

During the last three decades the sea ice area in the Arctic Ocean has shown a distinct decline. The largest reductions are found for the month of September when the annual minimum sea ice area is reached. Decline in sea ice area and thickness also result in a reduction of sea ice volume. Based on data from the laser altimeter on board ICESat, Kwok et al. (2009) found a net loss of 5400 km3 in October-November and 3500 km3 in February-March during the ICESat period from 2003 to 2008. Recent results, exploring new data from CryoSat-2, report a further decline in Arctic sea ice volume (Laxon et al., 2013; Tilling, 2016). The average sea ice volume in October-November for 2010 and 2011 was estimated to be 7560 km3, i.e. 64% of the 2003-2008 mean value estimated from ICESat (Kwok et al., 2009). However, all these findings are associated with large uncertainties.

9.3 Sea level change

Most of the Arctic Ocean is covered with sea ice which varies in extend and thickness on seasonal to interannual time scales with a distinct decrease in ice coverage and sea ice thickness during the recent decades as mentioned in section 9.2 and reported by Laxon et al., (2013); Kwok et al., (2009); and Tilling, (2016). Armitage et al (2016) performed an EOF analysis of monthly retracked ENVISAT data to inspect the dominant modes of seasonal and non-seasonal Artic SSH variability. They first computed the EOF on the full SSH and concluded that the leading two modes account for 62.6% of the variance. They next removed the mean seasonal cycle and re-performed the EOF analysis on the non-seasonal SSH variability. The result is shown in Figure 9.4.

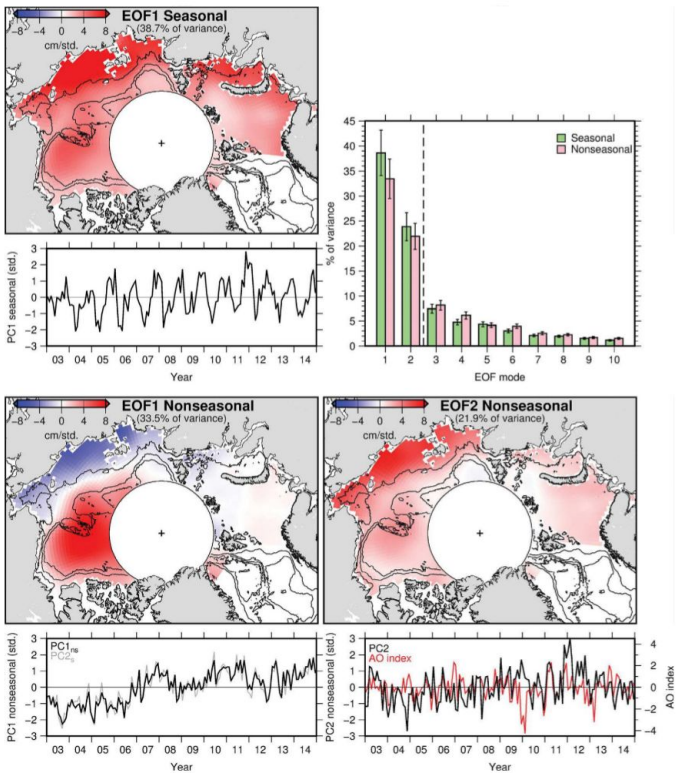

***Figure 9.4**. The dominant modes of seasonal and non-seasonal Arctic SSH variability from Envisat. The leading seasonal EOF is shown in the upper left figure. The upper right figure shows the variance explained by the first seasonal and first non-seasonal mode. The leading two EOFs of the non-seasonal SSH field are shown in the lower two figures. The AO is superimposed on the second non-seasonal EOF. Also contours of bathymetry is shown in the pictures.*

Armitage et al. (2016) concluded that the Arctic SSH variability is dominated by the seasonal cycle and that the seasonal EOF1 captures 38.7% of the total SSH variance. In comparison, the non-seasonal EOF analysis is dominated by secular changes capturing 33.5% of the variance. The second EOF2 is dominated by wind stress being largest along the Siberian shelf seas and accounting for 21.9% of non-seasonal SSH variance. Peralta-Ferriz et al. (2014), moreover, found that this mode of variability was significantly correlated with the Arctic Oscillation (AO) index (www.cpc.noaa.gov). A positive AO index indicates low atmospheric pressure over the central Arctic Ocean, which is responsible for driving the eastward alongshore wind anomalies in the Siberian Arctic (Peralta-Ferriz et al., 2014). Variations in sea level pressure and winds are also largely responsible for sea-ice drift in the Arctic.

9.3.1 The Seasonal cycle

The seasonal cycle detected by Armitage et al., (2016) using EOF analyses can also be explored from the 20-year DTU-SSH dataset augmented with the estimation from Cryosat-2 north of 82°N as shown in Figure 9.5. The seasonal cycle has a near uniform phase throughout the Arctic Ocean with maximum in October-December and a minimum in May-June (Fig 9.5, left, center). The largest amplitudes reaching 10 cm are found on the Siberian shelf. This amplitude clearly decreases to a few cm pole-ward toward the central area of the Arctic Ocean.

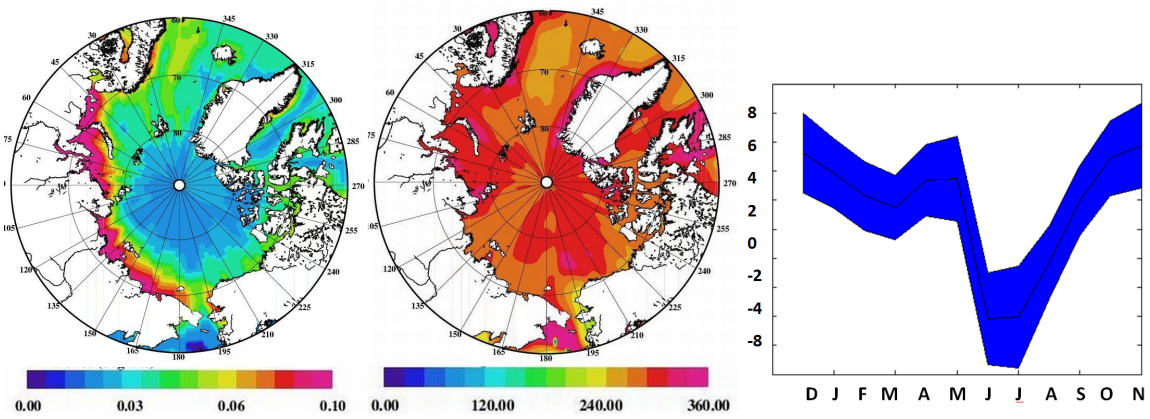

Figure 9.5*. The seasonal SSH signal in the Arctic Ocean derived from satellite altimetry with the amplitude (left), phase (center) and basin average with the associated uncertainty estimate (right). The amplitude in the left figure is given in meters and in cm in the right figure. The amplitude in the central figure is given in degrees.*

The basin-averaged mean Arctic SSH seasonal cycle shows a broad maximum of 4-5 cm between October–January, and a minimum of -4 cm in June-July. A secondary maximum of nearly 4 cm is also seen in April-May. Smaller intermediate peaks noticed in ocean mass data and have previously been linked to the annual cycle of river runoff (Peralta-Ferriz and Morison, 2010).

The large annual signal in the Arctic Ocean provides a challenge for tidal modelling using satellite altimetry. With only sun-synchronous satellites being available in the Arctic, the problem is that the diurnal constituents K_1 and P_1 have alias periods of exactly one year (365 days) when observed by the altimeter satellites. As such they are inseparable from the seasonal cycle. Similarly the semidiurnal constituent K_2 tidal constituent has an alias period of 183 days, which makes it inseparable from the semi-annual signal (S_{sa}). Although this signal generally has less amplitude in the Arctic Ocean it adds to modify the highs and lows in the annual variation due to e.g., the large fluxes of freshwater in and out of the Arctic Ocean.

The phase of the SSH seasonal cycle from altimetry is fairly similar to that observed directly by tide gauges (Proshutinsky et al., 2004; Richter et al., 2012). However, the amplitude is somewhat smaller. This is partly explained since the tide gauges measure SSH variations closer to the coast (compared to the altimeters) where the seasonal cycle is largest and where the persistent seasonal ice-coverage will limit the satellite altimetry.

Another explanation for the differences in the observed amplitude is the fact that the tide gauges observe the real variations in the sea level including the variations caused by the atmospheric pressure effect. Satellite altimetry, in contrast, is corrected for the atmospheric pressure effect via the inverse barometer effects. This inverse barometer correction (Wunch and Stammer, 1997) also frequently called Dynamic Atmosphere Correction corrects for the hydrostatic response to surface pressure variations. The altimeter SSH signals examined without applying the inverse barometer effect are therefore yielding a more direct comparison to tide gauges data. This is shown in Figure 9.6 for the seasonal SSH amplitude (left) and phase (center). As expected, the structures reveal distinct differences from the patterns shown in Figure 9.6. The sea level pressure is therefore clearly contributing to the seasonal to inter-annual variations in SSH. This is further documented by the averaged Arctic Ocean sea level pressure changes derived over several decades and reported by Thorndyke, (1982). In Figure 9.6 (right) significant variations in SSH are displayed throughout the Arctic Ocean. On average the amplitude of the sea level pressure is 4 mb which roughly corresponds to 4 cm in sea level.

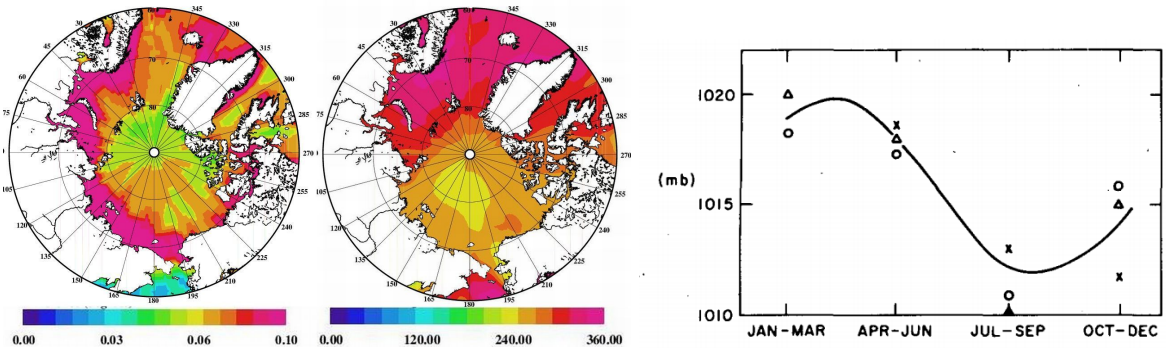

***Figure 9.6**. The seasonal SSH signal in the Arctic Ocean derived from satellite altimetry without applying for the inverse barometer correction. The amplitude in the left figure is given in meters. The amplitude in the central figure is given in degrees. To the right the Arctic-wide averaged sea-level pressure from Thorndyke (1982) is shown. Data from various years (triangles, crosses and circles) are shown.*

Throughout the ocean the amplitude of the seasonal cycle is increased and again the largest amplitudes around found along the Siberian shelves. The analysis also indicate that the presence of sea level pressure shifts the peak of the annual signal in sea level slightly later in the season (towards November) in the Northern Atlantic Ocean and slightly earlier in the interior of the Arctic Ocean. The latter shift inside the Arctic Ocean should be considered with caution as the non-inverted barometer data were obtained from the RADS which has very few data here.

9.3.2 Secular and long term sea level changes

Several studies have dealt with the linear sea level trend over the altimetry era. Prandi et al. (2012) reported 3.6+/− 1.3 mm/yr trend from reprocessed altimetry and 2.2 +/− 1.3 mm/yr using standard AVISO dataset over the 1993-2009 period while Scharroo et al. (2006, personal communication) estimated mean sea level drop in the Arctic Ocean over the 1996–2003 of 2 mm/yr. Figure 9.7 shows the averaged sea level variations over the last 23 years (blue) with a 1-year moving average superimposed in order to remove the annual sea level variations. The regional sea level trend computed over the period 1993-2015 indicates an increase of 2.2 ± 1.1 mm/y, which is relatively consistent with the results obtained by Svendsen (2015).

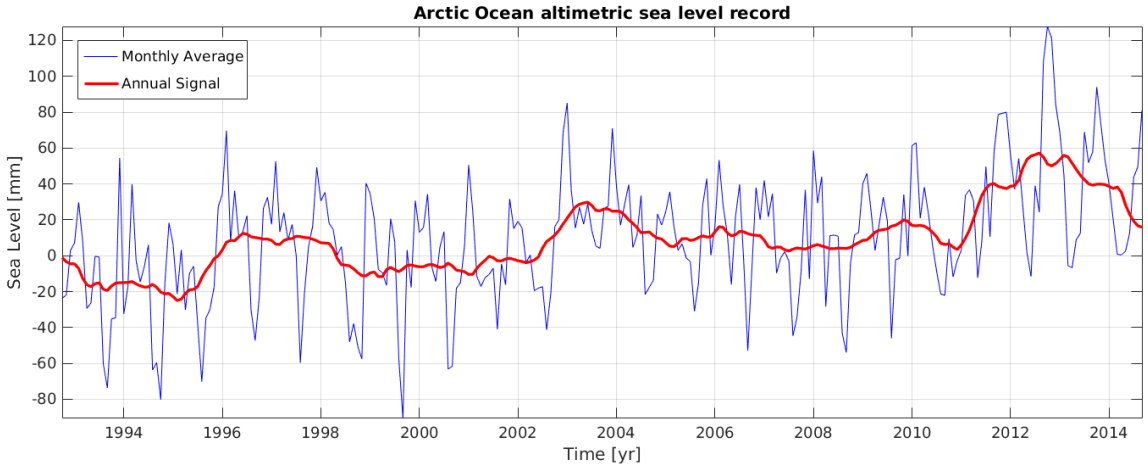

***Figure 9.7**: Regional sea level variations over 1993-2015. Monthly values (blue curve) are averaged with a 13-month moving mean (red curve).*

Large inter-annual variations in sea level variability is seen in the Arctic Ocean linked to the Arctic Oscillation (AO) and sea level pressure as revealed by a study on Arctic Ocean Model Intercomparison project reported by Prochutinsky et al., (2007). The averaged Arctic sea level curve also exhibit large inter-annual variation and shorter averaging period reveals both period of sea level increase and sea level drop. Interesting enough the sea level drop found by Scharroo et al., 2006) for

the 1995-2003 period is also found here with a similar negative trend of 1.8 mm/year. A detailed view of spatial pattern of the linear sea level trend for period 1993-2015 is presented in Figure 9.8 (left) with a spatial resolution of 1°x1°.

Changes in SSH reflect changes in volume and mainly increase or decrease in storage of freshwater in the Arctic. The increased sea level confirms the findings from moorings, ships and Ice-Tethered Profilers (ITPs) that the Arctic has accumulated up to 10,000 km3 of freshwater during the 1990s and 2000s ((Proshutinsky et al., 2009; Krishfield et al., 2014; Rabe et al., 2014). The SSH trend pattern is dominated by a significant positive trend in the area of the Beaufort Sea, where an increase of almost 15mm/y is registered (Figure 9.8 right). This is due to the Beaufort Gyre, a wind driven phenomenon that leads to freshwater accumulation (Rabe et al., 2011). Giles et al. (2012) estimated that the Beaufort Gyre accumulated 8000 ± 2000 km3 of freshwater in the 2000s and Bulczak et al. (2015) associated that with a change in sea level of roughly 2 mm/year.

In the northern part of the Nordic Seas and the Barents Sea we observe regional sea level trend of 3-5 mm/years, which is comparable to what is seen by i.e., Nerem et al. (2010). Very close to the east coast of Greenland the high sea level trend is questionable and can be attributed to the fact that few data exist during the ERS-1/ERS-2/ENVISAT period due to heavy sea ice coverage whereas in the same area Cryosat-2 provides a very narrow strip of SAR-in data.

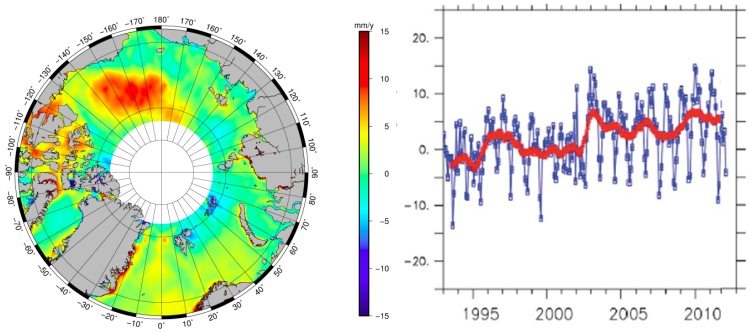

***Figure 9.8**: Spatial pattern of linear sea level trend for the 1993-2015 period. The figure to the right shows the sea level averaged over the Beaufort gyre bounded by longitudes 150°E and 240°E.*

In order to extend the studies of sea level change in the Arctic Ocean beyond the altimetry era to longer periods it is important to use a careful selection of tide gauges. *Proshutinsky et al*. (2004) used tide gauges to estimate a secular sea level change in the Siberian Arctic of 1.85 mm/yr between 1954 and 1989, while *Richter et al*. (2012) estimate trends of 1.3–2.3 mm/yr along the Norwegian coast between 1960 and 2010. Reconstructing historical Arctic Ocean sea level change is also highly challenging, due to the relatively small amount of usable data. In a recent paper by Svendsen et al., 2016, the datum-fit sea level reconstruction method (Ray and Douglas) produces very stable Arctic linear sea level trend of around 1.5 +/-0.3mm/y for the period 1950 to 2010, between 68ºN and 82ºN (see Figure 9.9). This value is also in good agreement with the global mean trend of 1.8+/- 0.3 mm/y for 1950–2000, as reported by Church et al. (2004).

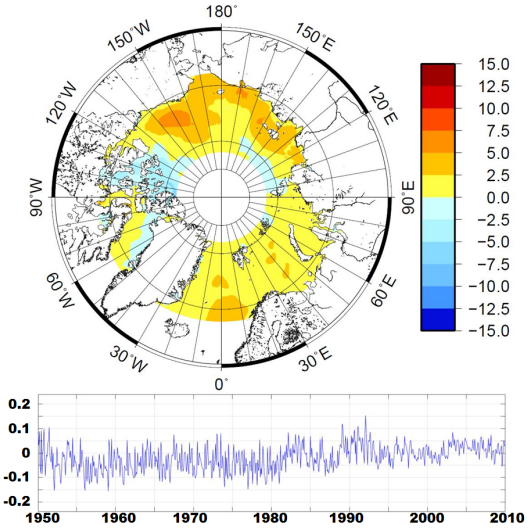

***Figure 9.9**: Reconstructed linear sea level trend for the 1950-2009 period. The values in the upper figure is given in mm/year whereas the monthly averaged sea level for the period in the lower figure is given in meters.*

9.3.3 Arctic Sea level budget

The sea level budget equation in its most simple form reads:

$$\mathbf{\Delta S_{sl} = \Delta S_{mass} + \Delta S_{steric}}$$

Where ΔS_{sl} is the observed sea level, ΔS_{mass} is the ocean mass variation and ΔS_{steric} is the steric component. Smaller contributions due to inflow and outflow from the Arctic Ocean as well as the sea level pressure variations should be accounted in the overall sea level budget. However, as a first estimate these contributions can be neglected. The Arctic budget closure can be evaluated by comparing the updated sea level record with GRACE EWT ocean mass solution (Watkins et al., 2015) with estimates of steric sea level provided by NOAA Ocean Heat and Salt content dataset (NOAA, 2014). GRACE ocean mass variations are processed without accounting for the atmospheric pressure component. This correction is therefore applied using the ECMWF ERA-Interim model, and integrated according to Wunsch and Stammer (1997). The sampling and resolution of the NOAA halo- and thermos-steric data as well as the coverage of the input data are very sparse during the 2003-2015 period (Andersen and Piccioni, 2015). As such the estimates are associated with considerable uncertainties. Furthermore in order to obtain consistency between the GRACE ocean mass and NOAA steric estimates the data were truncated at 82°N to reflect the coverage of the altimetry data.

For the period 2003-2015 Andersen and Piccioni (2016) found an altimetric sea level rise of 4.3 +/- 2.4 mm/y, while GRACE EWT registers an increase in ocean mass corresponding to a sea level rise of 3.9 mm/y +/- 0.9 mm/year. The thermo- and halo-steric each contributes to 0.3 mm/year but with different sign implying that the total steric trend is insignificant during this 12-year period.

9.3.4 The Polar gap and accuracy estimates

Since as much as 27% of the Arctic Ocean is not covered by the ERS-1, ERS-2 and ENVISAT altimeters the estimates are considered to be biased significant uncertainty. Similarly large regions of the Arctic Ocean will have large voids in the temporal resolution - even after retracking. Temporal voids in the altimeter record will cluster during the winter month for particularly conventional satellites biasing the estimate of the annual variation. With Cryosat-2 a significant step forward have been made in terms of temporal and spatial sampling of the Arctic Ocean and this satellite now covers more than 96% of the entire Arctic Ocean and the temporal sampling is hugely increased with significantly more data from leads in the ice during winter and in regions with near permanent ice

coverage. However, since Cryosat-2 was only launched in 2010 observations of long-term changes north of 82N are still to come.

Recently, Armitage et al. (2016) investigated the effect of the Polar gap using Cryosat-2 data in which monthly mean SSH was calculated using; (i) all CryoSat-2 data south of 88°N, and (ii) just data south of 81.5°N. In so doing the impact of the inclusion of data north of 81.5°N on the basin mean estimates could be determined. They achieved very good correlation between month-to-month variations north and south of 81.5°N, giving confidence to the fact that temporal variations in mean SSH south of 81.5°N are representative of variations across the whole basin at monthly to seasonal time scales. For long-term changes, on the other hand, the situation is more challenging. The net accumulation across the Arctic Basin will be partly missed by the polar gap in satellite altimetry. Whereas the Beaufort Gyre is mostly within the coverage of the ERS-1, ERS-2 and ENVISAT satellites, there are periods during when the Gyre extends north of 82° N. For instance, ERS-2 and ENVISAT both captured the changes in SSH and freshwater content in the Canada Basin between 2004 and 2008. However, the satellite altimeters did not observe the changes in the SSH north of 81.5° as reported by Kwok and Morison, (2012). They used the ICESat data to compute the mean dynamic topographies for each of the ICESat winter campaigns during the same period, and detected significant variations associated with the Beaufort Gyre north of 82N as shown in Figure 9.10.

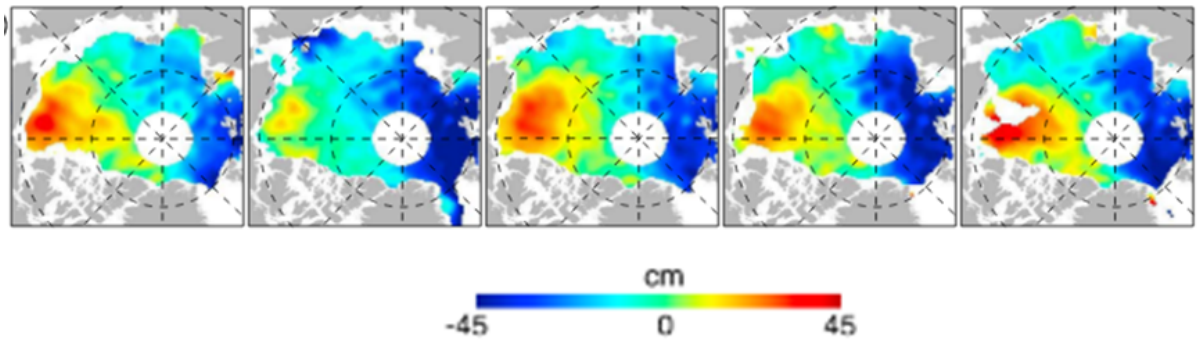

Figure 9.10. *Mean Dynamic Topography from ICESat for each of the winters 2004-2008 from Kwok and Morrison (2012) illustrating how the Beaufort Gyre anomaly extends outside the coverage of the ERS / ENVISAT satellites.*

9.4 Mean dynamic topography

The dynamic topography can be interpreted in terms of influences from the water mass properties, ocean currents, ocean-atmosphere fluxes, and near surface winds. The time mean of the dynamic ocean topography is called the Mean Dynamic Topography (MDT). This reflects the long-term dynamically driven departure of the sea surface height (SSH) from the geoid which is represented by the mean sea surface (MSS). In turn, the time-mean ocean geostrophic current is estimated from the corresponding slope of the MDT (= MSS - h_{geoid})

The MDT is derived with respect to the temporal averaging period over which the corresponding MSS is derived from satellite altimetry. The time-mean used to calculate the surface geostrophic currents and ocean transports is particularly sensitive to geoid residuals, since accurate models of the gravitational field are required to separate the marine geoid and oceanographic signals.

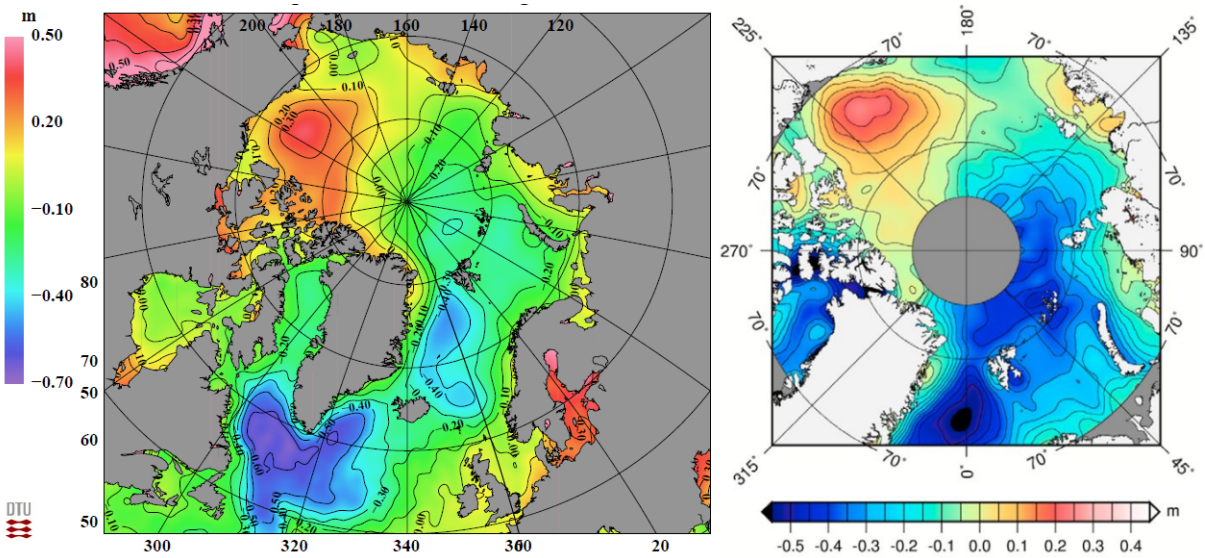

Figure 9.11. *Two independent MDT models for the Arctic Ocean. (left)The DTU15MDT derived from the DTU15MSS and the EIGEN6-C4 geoid model. (right) The MDT by Farrell derived from ICESat. The grey sector centered at the Pole marks lack of coverage.*

The main features of the Arctic MDT (DTU15MDT) derived from the new DTU15MSS and the EIGEN6-C4 (Figure 9.11) are, as expected, consistent with Johannessen et al., (2014) and clearly reveals the presence of: a high (> 0.3 m) in the Beaufort Sea associated with the anticyclonic Beaufort Gyre; a large-scale slope (~ 0.6 m/1300 km) in topography from the Amerasian Basin to the Eurasian Basin associated with both the Beaufort Gyre and transpolar current; a low (< - 0.2 m) in the Norwegian and Greenland Seas associated with the cyclonic circulation; the expression of a sloping MDT (~ 0.4 m/500 km) in the northeast Atlantic consistent with the North Atlantic Current and its extension to the Norwegian North Atlantic Current; and a distinct low (< - 0.6 m) in the Sub-Polar gyre connected with the circulation in the north Atlantic and Labrador Sea. These findings and results are also agreeing qualitatively well with previous and recent results derived from satellite altimetry (Kwok and Morison, 2011; Farrell et al., 2012; Giles et al., 2012; Kwok and Morison, 2015) as well as from ocean models (e.g., Koldunov et al., 2014; Proshutinsky et al., 2015). In the Nordic Seas, moreover, the spatial pattern in the MDT also agrees well with the spatial pattern in the mean steric height derived from hydrographic data (Nilsen et al. 2008) for the period 1950–2010 as shown by Johannessen et al., (2014).

In the recent work by Kwok and Morison (2015), the time-mean dynamic topography (MDT) from ICESat (Kwok and Morison, 2011), CS-2 DOT2008A (Andersen and Knudsen, 2009, Pavlis et al, 2012), and DTU13MDT (Andersen et al., 2015) are compared primarily for the Arctic Ocean (Figure 9.12). The MDTs are smoothed with a 250 km Gaussian averaging-kernel to reduce the noise in the SSH measurements and the contribution of residual geoid errors at shorter wavelengths. Although the ICESat and Cryosat-2 MDTs are from different epochs with potential biases between the two instruments, their spatial patterns are comparable and in agreement with Johannessen et al., (2014) with a well-defined dome in the Canada Basin located to the Beaufort Sea and an east-west gradient across the Amerasian and Eurasian Basins. The spatial MDT patterns are also agreeing with main features of the Arctic MDT derived from the DTU15MDT as shown in Figure 9.11.

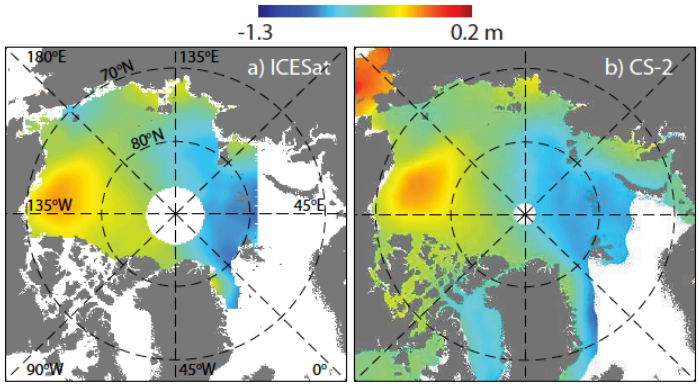

Figure 9.12. *Mean dynamic topography of the ice-covered Arctic Ocean. (a) ICESat (Mean of Feb-Mar, 2003-2008) (Kwok and Morison, 2011), (b) CryoSat-2 (2011-2014). The fields have been smoothed with a 250-km Gaussian kernel.*

9.5 Ocean circulation and volume Transport

9.5.1 Surface circulation

There are two main pathways by which the Arctic Ocean connects with the global ocean circulation (Figure 9.1), notably the Pacific-Arctic Ocean and the Atlantic-Arctic Ocean gateways (Rudels and Friedrich 2000). The Pacific-Arctic Ocean gateway is the narrow (~ 85km wide), shallow (~ 50m deep) Bering Strait, through which about 0.8Sv (1Sv=10^6m^3/s) of water enters the Arctic. Properties of this inflow display significant seasonal variability, from about 0.4Sv, -1.9ºC, and 33 psu in winter to about 1.2Sv, greater than 2ºC, and less than 31.9 psu in summer (Woodgate *et al.* 2005a). The Atlantic-Arctic Ocean gateway is through both the Fram Strait (~ 350km wide, ~ 2700m deep) and the Barents Sea (mostly via St Anna Trough, ~ 200km wide, ~ 600m deep). The Atlantic inflow is generally saltier (greater than 34 psu), warmer (greater than 0ºC), and about 10 times greater in volume than the Pacific-Arctic Ocean inflow (Beszczynska-Möller *et al*. 2011). The Fram Strait inflow is about 7Sv and varies seasonally (Fahrbach *et al.* 2001), although complex recirculations in the Fram Strait return around half of the inflow (Rudels *et al.* 2000b). The Barents Sea inflow is around 1Sv in summer and 3Sv in winter, and is substantially modified during the transit across the Barents Sea (Schauer *et al.* 2002a).

The other inputs to the Arctic Ocean are volumetrically small: Eurasian and Russian rivers (~ 0.1Sv) and precipitation minus evaporation (~ 0.06Sv). However, together they contribute roughly two-thirds of the freshwater entering the Arctic Ocean, the remaining third coming from the Pacific inflow (Aagaard and Carmack 1989, Serreze *et al.* 2006).

The outflows from the Arctic Ocean, on the other hand, are all to the North Atlantic Ocean, either through the western side of the Fram Strait (~ 9Sv, Fahrbach, *et al.* 2001), or via the complex channels of the Canadian Archipelago (~ 1-2Sv, Melling *et al.* 2008). All these inflow and outflow estimates are approximate, with uncertainties typically ranging around 25% as pointed out in the review paper by Beszczynska-Möller *et al*. (2011).

Within the Arctic Ocean the circulation is characterized by the eastward flowing Atlantic water in the Eurasian basin, the transpolar drift from the Siberian shelf region to the Fram Strait and the clockwise circulation in the Beaufort Gyre in the Canadian Basin as illustrated in Figure 9.1. The distinct development and presence of the dome in the Beaufort Gyre from 2003 to 2014 is primarily connected and influenced by the atmospheric wind field and ocean circulation in the Arctic Ocean. For the period 2005 to 2009 Koldunov et al., (2014) suggest that an anomalous transport (referenced to the 1970-2000 mean transport) in the upper ocean driven by dominant negative anomalies in the Ekman pumping that directed fresh Siberian, Alaskan and Canadian Archipelago shelf and upper slope waters into the Beaufort Gyre as shown in Figure 9.13. This led to a convergence of low salinity water and subsequent increase of the steric height and hence formation of the dome as expressed in the MDTs

depicted in Figures 9.10, 9.11 and 9.12.

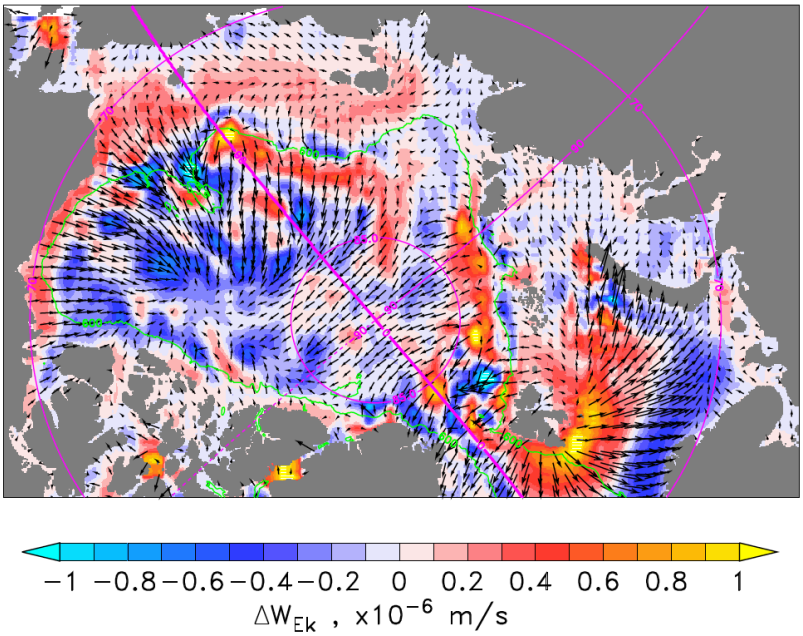

Figure 9.13. *Ekman pumping anomaly (2005-2009 average minus 1970-2000 average) with the respective anomaly of Ekman transports superimposed (largest vector = 0.2 m2 s−1) computed from the ATL12 wind stress. The isobath shown by the green line corresponds to 600 m depth.*

Within the Greenland-Island-Norwegian (GIN) Seas the mean surface geostrophic velocities (Figure 9.14) are computed from the GOCE MDT for the period 1993-2009 in consistence with the period for the construction of the DTU MSS data, wh by:

$$u_s = \frac{-g}{f} \cdot \frac{\partial MDT}{\partial y|}$$

$$v_s = \frac{g}{f} \cdot \frac{\partial MDT}{\partial x}$$

Here u_s and v_s are components of the surface geostrophic velocity, g is the acceleration due to gravity, f is the Coriolis parameter, and x and y are the zonal and meridiornal directions. The large-scale cyclonic surface circulation regime is well reproduced with the inflowing Atlantic Water to the Norwegian Sea reaching nearly 0.2 m/s. The broadening of the Norwegian Atlantic Current (NwAC) over the Vøring Plateau and in the Lofoten Basin is also noticed, as is the northward flowing West Spitsbergen Current (WSC) and the strong southbound East Greenland Current (EGC). When the altimeter-based SLA is added to the MDT these branches appear strongest in wintertime in consistence in-situ bas bservations reported by Mork and Skagseth, (2005).

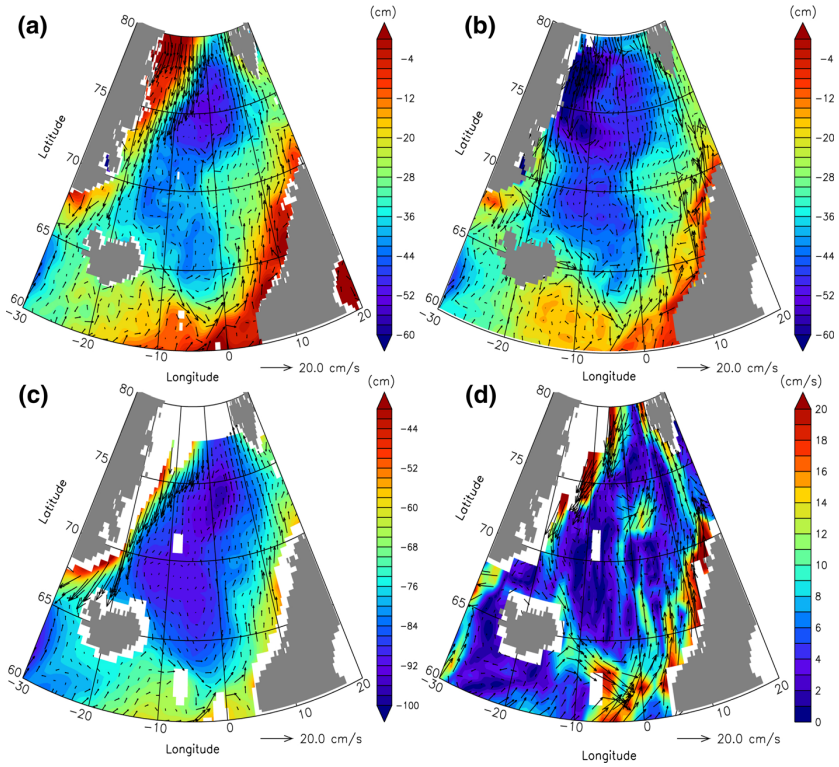

Figure 9.14. *Mean surface geostrophic velocities vectors superimposed on the mean dynamic topography (MDT) derived from a GOCE, b CNES_CLS09, c Maximenko et al. (2009), and d mean surface velocity vectors derived from the climatology of the global surface drifter data. Color scale indicates the MDT in cm for (a) to (c) and speed in cm/s for (d). Current-vector scale shown in the lower right corner. (Courtesy Johannessen et al., 2014.)*

9.5.2. Volume transport

By combining the GOCE derived MDT and altimetric sea level anomalies (SLA) with the comprehensive hydrographic data base (Johannessen et al., (2014) estimated the mean and variable transport of Atlantic Water (salinity >35) entering the Nordic seas for the period 1993 – 2011 at a spatial resolution of 100 km. Using 44 CTD-sections for the Island-Faroe Ridge (IFR), 84 CTD-sections for the Faroe-Shetland Channel (FSC) and 76 CTD-sections taken along the Svinøy section the baroclinic velocity structures in the Atlantic Water were estimated across these sections. Combined with the barotropic velocity values the absolute velocities are then retrieved, and when multiplied to the area covered by the Atlantic Water estimates of the corresponding volume transports of Atlantic Water across the 3 sections are obtained and compared to previous observations and simulation as given in Table 9.2.

Source	Data	Period	IFR (Sv)	FSC (Sv)	Svinøy (Sv)		
					NwAFC	NwASC	Total
Johannessen et al., (2014)	GOCE + Altim. + hydr.	1993-2011	3.5	4.1	3.0	3.9	6.9
Mork and Skagseth (2010)	Altim. + hydr.	1993-2009			1.7	3.4	5.1
Skagseth et al. (2008)	current meter	1995-2006				4.3	
Orvik and Skagseth (2005)	curr. meters	1995-1999				4.2	
Orvik and Skagseth (2003)	curr. meters	1998-2000				4.4	
Orvik et al. (2001)	curr. meters + ADCP + hydr.	1995-1999			3.4	4.2	7.6
Berx et al. (2013)	Altm.+ADCP+hydro	1995-2009	3.5				
Østerhus et al. (2005)	Bottom ADCP + hydr.	1999-2001	3.8	3.8			
Hansen et al. (2010)	Bottom ADCP + hydr.	1997-2008	3.5				
Hansen et al. (2003)	Bottom ADCP + hydr.	1997-2001	3.5				
Sandø et al. (2012)	MICOM model	1994-2007	4.7*	4.7			
Johannessen et al., (2014)	MICOM model	1993-2007	3.5	6.9	3.5	5.0	8.5
Johannessen et al., (2014)	ATL model	1993-2007	3.5	4.2	3.5	4.7	8.2

Table 9.2. *Comparison of volume transport estimates from combined GOCE, altimetry and in-situ data to previous studies as well as estimates from simulation models for the Island-Faroe Ridge (IFR), Faroe-Shetland Channel (FSC), NwAFC, NwASC in the Svinøy Section and the total Svinøy Section. (* only from 1997-2007.)*

The mean inflows of Atlantic Water across the IFR and through the FSC are estimated to 3.5 Sv and 4.1 Sv respectively (1 Sv = 10^6 m^3s^{-1}). Moreover, the mean transport of the two branches of Atlantic Water crossing the Svinøy section, e.g. the Norwegian Atlantic Slope Current (NwASC) and the Norwegian Atlantic Front Current (NwAFC) is respectively 3.0 Sv and 3.9 Sv. These estimates compare reasonably well with the earlier reported observed and simulated transport values despite the different integration periods. However, discrepancies exist including the total combined GOCE-, altimeter- and hydrographic-based transport estimates across the Svinøy section that is about 20% lower than the simulated transports (e.g. 6.9 Sv versus 8.5 and 8.2 Sv). According to Johannessen et al., (2014) this is partly related to the definition and choice of layers for the Atlantic Water transport estimations. These disagreements in transport estimates imply significant differences in the mean northward advection of heat and salt to the Nordic Seas and Arctic Ocean. This, in turn, may affect both the evaporation-precipitation fluxes and convective overturning in the Norwegian and Greenland Seas.

Taking benefit of the temporal variability observed in the altimeter SLA and the hydrographic data the mean and seasonal cycle in the transport of the inflowing Atlantic Water for the period 1993 to 2009 can also be estimated and inter-compared as shown in Figure 9.15 for the Svinøy section. The mean seasonal variability reveals a pattern with largest transports (9.3 Sv) in winter compared to the summer transport minimum (5.4 Sv). Moreover, the mean seasonal NwASC transport always exceeds the mean seasonal NwAFC transport, while the latter display a narrower range of seasonal variability in the volume transport. This suggests that the seasonal changes of the transport across the Svinøy section are predominantly controlled by seasonal changes in the transport of the NwASC.

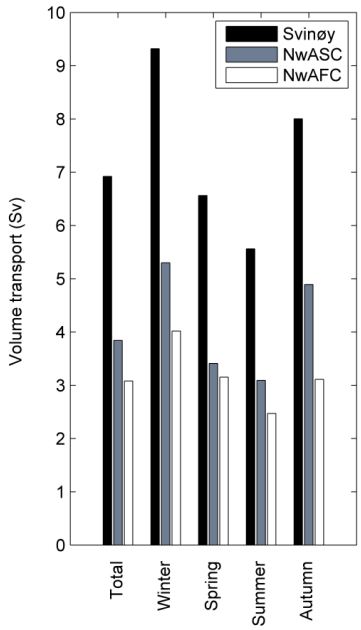

Figure 9.15. *Mean annual and mean seasonal total volume transport estimates for the Svinøy section (black) compared to the mean transports of the NwASC (grey) and the NwAFC (white) for the period 1993-2011 based on combined use of GOCE, altimetry and in-situ hydrography data.*

Altogether, these GOCE-based estimates combined with altimeter-based SLA and in-situ hydrographic data are providing new and promising abilities to examine the seasonal transport variability (total as well as barotropic and baroclinic components) across key selected regions. As such, it is also providing an important tool for validations of modelsand simulation of transports between the Northeast Atlantic Ocean, the Nordic Seas and Arctic Ocean.

9.6 Summary and Outlook

Satellite altimetry is fundamental to monitor sea level and its changes on various time scales in the Arctic Ocean. Availability of data sources such as in situ observations, satellite altimetry, GOCE- and GRACE-based gravity fields enables the derivation of Mean Dynamic Topographies which put valuable constrains on both the use of satellite altimetry and ocean modelling.

The success of ICESat has paved the way for the use of laser altimetry for sea ice thickness retrievals in the Arctic Ocean and soon a continuation of ICESat-2 will enable ultra-high resolution surface mapping. Moreover, the availability of SAR altimetry from Cryosat-2 has advanced the multidisciplinary studies of the Arctic Ocean dynamics and mean sea level, variability in the sea ice thickness and volume, and the distribution of leads.

In addition, the success of the Cryosat-2 SAR altimetry enabled the important decision to maintain continuity of SAR altimetry observations in the Arctic Ocean from the Sentinel-3 (A/B) satellites for the next decade at an inclination of 98.65°. Moreover, within a few years the Surface Water Ocean Topography (SWOT) satellite will be launched and provide high resolution (15 km) SAR-in in the Arctic Ocean. However, the inclination of the SWOT mission will only be 78°. Hence Sentinel-3 and SWOT will lack between 27% and 35% coverage of the northern most sector of the Arctic Ocean.

However, for studies of the Arctic Ocean sea ice thickness and sea level as well as monitoring of freshwater storage in the Arctic Ocean a continuation of the Cryosat-2 mission is fundamentally important such as eventually with a dual frequency all interferometric mission called Cryosat-3. By measuring in both Ku- and Ka-band such a mission concept will also be able to map the snow depth on the sea ice in the Arctic Ocean, a major contributor to the uncertainty in sea ice freeboard and sea ice thickness retrievals.

References

Aagaard, K., and E. Carmack (1989), The role of sea ice and other fresh water in the Arctic circulation, J. Geophys. Res., 94, 14,485–14,498,doi:10.1029/JC094iC10p14485.

Ablain, M., A. Cazenave, G. Larnicol, M. Balmaseda, P. Cipollini, Y. Faugère, M. J. Fernandes, O. Henry, J. A. Johannessen, P. Knudsen, O. Andersen, J. Legeais, B. Meyssignac, N. Picot, M. Roca, S. Rudenko, M. G. Scharffenberg, D. Stammer, G. Timms, and J. Benveniste (2015), Improved Sea Level record over the satellite altimetry era (1993-2010) from the Climate Change Initiative project, *Ocean Sci., 11, 67–82,* doi:10.5194/os-11-67-2015.

Andersen, O. B., and Knudsen, P. (2009) The DNSC08 mean sea surface and mean dynamic topography models, J. Geophys. Res., doi:10.1029/2008JC005179

Andersen, O. B. and G. Piccioni (2016) Recent Arctic Sea Level Variations from Satellites, Frontiers in Marine Science, 3, journal.frontiersin.org/article/10.3389/fmars.2016.00076, DOI=10.3389/fmars.2016.00076

Andersen, O., P. Knudsen, and L. Stenseng (2015), The DTU13 MSS (Mean Sea Surface) and MDT (Mean Dynamic Topography) From 20 Years of Satellite Altimetry, pp. 1–10, Springer, Berlin, doi:10.1007/1345_2015_182.

Armitage, T. W. K., S. Bacon, A. L. Ridout, S. F. Thomas, Y. Aksenov, and D. J. Wingham (2016), Arctic sea surface height variability and change from satellite radar altimetry and GRACE, 2003–2014, J. Geophys. Res. Oceans, 121, 4303–4322, doi:10.1002/2015JC011579.

Bamber, J., M. van Den Broeke, J. Ettema, J. Lenaerts, and E. Rignot (2012), Recent large increases in freshwater fluxes from Greenland intothe North Atlantic, Geophys. Res. Lett., 39, L19501, doi:10.1029/2012GL052552.

Belkin, I. (2004), Propagation of the ‘‘Great Salinity Anomaly’’ of the 1990s around the northern North Atlantic, Geophys. Res. Lett., 31,L08306, doi:10.1029/2003GL019334.Prog. Oceanogr., 20, 103–151, doi:10.1016/0079-6611(88)90049-3.

Cheng, Y., and Andersen, O. B. (2011) Multi-mission empirical ocean tide modeling for shallow waters and polar seas. J. of Geophys. Res., 116(C11), 1-11, doi: 10.1029/2011JC007172

Cheng Y., Andersen O. B., Knudsen P. (2015). An Improved 20- Year Arctic Ocean Altimetric Sea Level Data Record, Marine Geodesy, 38:2, 146-162, DOI: 10.1080/01490419.2014.954087

Church, J. A. and White, N. J. (2011). Sea-level rise from the late 19th to the early 21st century. Surv. Geophys., 32(4-5):585–602.

Dickson, R. R., J. Meincke, S.-A. Malmberg, and A. J. Lee (1988), The ‘‘Great Salinity Anomaly’’ in the northern North Atlantic 1968–1982, Prog. Oceanogr., 20, 103–151, doi:10.1016/0079-6611(88)90049-3. Prog. Oceanogr., 20, 103–151, doi:10.1016/0079-6611(88)90049-3.

Farrell, S. L., D. C. McAdoo, S. W. Laxon, H. J. Zwally, D. Li, A. Ridout, and K. Giles (2012), Mean dynamic topography of the arctic ocean, *Geophys. Res. Lett.*, 39, L01601, doi:10.1029/2011GL050052.

Giles, K. A., S. W. Laxon, A. L. Ridout, D. J. Wingham, and S. Bacon (2012), Western Arctic Ocean freshwater storage increased by wind-driven spin-up of the Beaufort Gyre, *Nat. Geosci.*, 5, 194–197, doi:10.1038/ngeo1379.

Helland-Hansen and Nansen (1909) The Norwegian Sea. Bergen, Digital copy available from Nansen Centret.

Henry, O., P. Prandi, W. Llovel, A. Cazenave, S. Jevrejeva, D. Stammer, B. Meyssignac, and N. Koldunov (2012) Tide gauge based Sea level variations since 1950 along the Norwegian and Russian coasts of the Arctic Ocean; contribution of the steric component, J. Geophys. Res., 117, C06023

Holgate, S. J., A. Matthews, P. L. Woolworth, L. J. Rickards, M. E. Tamisiea, E. Bradshaw, P. R. Foden, K. M. Gordon, S. Jevrejeva, and J. Pugh(2013), New data systems and products at the Permanent Service for Mean Sea Level, J. Coastal Res., 29, 493–504, doi:10.2112/JCOASTRES-D-12-00175.1.

IPCC (2013), Climate Change 2013: The Physical Science Basis, 1535 pp., Cambridge Univ. Press, N. Y.

Johannessen, J. A., R. P. Raj, J. E. Ø. Nilsen, T. Pripp, P. Knudsen, F. Counillon, D. Stammer, L. Bertino, O. B. Andersen, N. Serra and N. Koldunov (2014) Toward Improved Estimation of the Dynamic Topography and Ocean Circulation in the High Latitude and Arctic Ocean: The Importance of GOCE, *Survey in Geophysics*, Springer, DOI 10.1007/s10712-013-9270-y.

Kern, S., K. Khvorostovsky, H. Skourup, E. Rinne, Z. S. Parsakhoo, V. Djepa, P. Wadhams and S. Sandven (2014), About uncertainties in sea ice thickness retrieval from satellite radar altimetry: results from the ESA-CCI Sea Ice ECV Project Round Robin Exercise, *The Cryosphere Discuss., 8, 1–44, 2014*, doi:10.5194/tcd-8-1-2014.

Khan, S. A., Aschwanden, A., Bjørk, A. A., Wahr, J., Kjeldsen, K. K., Kjær, K. H.(2015). Greenland ice sheet mass balance: a review, *Rep. Prog. Phys. 78 046801*

Koldunov, N. V., N. Serra, A. Kohl, D. Stammer, O. Henry, A. Cazenave, P. Prandi, P. Knudsen, O. B. Andersen, Y. Gao and J. A. Johannessen (2014) Multi-model Simulations of Arctic Ocean Sea Surface Height Variability in the Period 1970-2009, *Journal of Geophys. Res., Oceans* 2014; Volume 119.(12) s. 8936-8954, doi:10.1002/2014JC010170.

Krishfield, R. A., A. Proshutinsky, K. Tateyama, W. J. Williams, E. C. Carmack, F. A. McLaughlin, and M.-L. Timmermans (2014), Deterioration ofperennial sea ice in the Beaufort Gyre from 2003 to 2012 and its impact on the oceanic freshwater cycle, J. Geophys. Res. Oceans, 119,1271–1305, doi:10.1002/2013JC008 999.

Kwok, R., and J. Morison (2011), Dynamic topography of the icecovered Arctic Ocean from ICESat, *J. Geophys. Res.*, **38**, L02501, doi:10.1029/2010GL046063.

Kwok, R., and J. Morison (2015), Sea surface height and dynamic topography of the ice-covered oceans from CryoSat-2: 2011–2014, *J. Geophys. Res. Oceans*, **121**, 674–692, doi:10.1002/2015JC011357.

McAdoo, D. C., S. L. Farrell, S. Laxon, A. Ridout, H. J. Zwally, and D. Yi (2013), Gravity of the Arctic Ocean from satellite data with validations using airborne gravimetry: Oceanographic implications, *J. Geophys. Res. Oceans, 118, 917–930*, doi:10.1002/jgrc.20080.

Morison, J., R. Kwok, C. Peralta-Ferriz, M. Alkire, I. Rigor, R. Andersen and M. Stele (2012), Changing Arctic Ocean freshwater pathways. Nature 481, 66–70, doi:10.1038/nature10705

NOAA (2015) https://www.nodc.noaa.gov/OC5/3M_HEAT_CONTENT/index.html.

Pavlis, N. K., S. A. Holmes, S. C. Kenyon, and J. K. Factor (2012), The development and evaluation of the Earth Gravitational Model 2008 (EGM2008), *J. Geophys. Res., 117*, B04406,

doi:10.1029/2011JB008916.
Peacock, N. R., and S. W. Laxon (2004). Sea surface height determination in the Arctic Ocean from ERS altimetry, J. Geophys. Res., 109, C07001, doi:10.1029/2001JC001026
Peralta-Ferriz, C., J. H. Morison, J. M. Wallace, J. A. Bonin, and J. Zhang (2014),Arctic Ocean circulation patterns revealed by GRACE, *J. Clim.*, 27,1445–1468, doi:10.1175/JCLI-D-13-00013.1
Prandi, P., M. Ablain, A. Cazenave, and N. Picot (2012). A new estimation of mean sea level in the Arctic Ocean from satellite altimetry, *Mar. Geod.,* 35, sup1, 61-81.
Proshutinsky, A. (2004) Secular sea level change in the Russian sector of the Arctic Ocean, *J. Geophys. Res.,* 109(C3), 1-19, doi:10.1029/2003JC002007
Proshutinsky, A., R. Krishfield, M.-L. Timmermans, J. Toole, E. Carmack, F. McLaughlin, W. J. Williams, S. Zimmermann, M. Itoh, and K. Shimada (2009) Beaufort Gyre freshwater reservoir: State and variability from observations, *J. Geophys. Res.,* 114, C00A10, doi:10.1029/2008JC005104
Proshutinsky, A, Ashik, I., Häkkinen, S (2007). Sea level variability in the Arctic Ocean from AOMIP models, *J. Geophys. Res.*, 112(C4), 1-25. doi:10.1029/2006JC003916
Richter, K., J. E. Ø. Nilsen, and H. Drange (2012) Contributions to sea level variability along the Norwegian coast for 1960-2010, J. Geophys. Res, 117(C5), 1-12. doi:10.1029/2011JC007826
Rabe, B., M. Karcher, U. Schauer, J. M. Toole, R. A. Krishfield, S. Pisarev, F. Kauker, R. Gerdes, and T. Kikuchi (2011) An assessment of Arctic Ocean freshwater content changes from the 1990s to the 2006–2008 period. Deep Sea Research Part I: Oceanographic Research Papers 58(2):173–185. doi: 10.1016/j.dsr.2010.12.002
Ray, R. D. and Douglas, B. C. (2011). Experiments in reconstructing twentieth century sea levels. Progress in Oceanography, 91(4):496–515.
Serreze, M. C., Barrett, A. P., Slater, A. G., Woodgate, R. A., Aagaard, K., Lammers, R. B.,... & Lee, C. M. (2006). The large-scale freshwater cycle of the Arctic. *Journal of Geophysical Research: Oceans (1978–2012)*, *111*(C11).
Serreze, M. C., and R. G. Barry (2011) Processes and impacts of Arctic amplification: A research synthesis, Global Planet. Change, 77, 85–96, doi:10.1016/j.gloplacha.2011.03.004.
Stroeve, J. C., V. Kattsov, A. Barrett, M. Serreze, T. Pavlova, M. Holland, and W. N. Meier (2012), Trends in Arctic sea ice extent from CMIP5,CMIP3 and observations, Geophys. Res. Lett., 39, L16502, doi:10.1029/2012GL052676.
Svendsen, P. L., Andersen, O. B., and Nielsen, A. A. (2015). Statistical selection of tide gauges for arctic sea-level reconstruction. Advances in Space Research, 55(9):2305–2314.
Svendsen, P. L. (2015). Arctic Sea Level Reconstruction, PhD diss., Technical University of Denmark
Thorndyke A. S. (1982). Statistical properties of the pressure field over the Arctic Ocean, J. Athmospheric Sciences, 39, 229-234.
Volkov, D., and F. W. Landerer (2013), Nons seasonal fluctuations of the Arctic Ocean mass observed by the GRACE satellites, J. Geophys. Res.,118, 6451–6460, doi:10.1002/2013JC009341.
Volkov, D. L., F. W. Landerer, and S. A. Kirillov (2013), The genesis of sea level variability in the Barents Sea, Cont. Shelf Res., 66, 92–104, doi:10.1016/j.csr.2013.07.007.
Volkov, D. L. (2014). Do the North Atlantic winds drive the nonseasonal variability of the Arctic Ocean sea level?, Geophys. Res. Lett., 41, 2041 – 2047, doi: 10.1002/2013GL059065
Watkins, M. M., Wiese, D. N., Yuan, D.-N., Boening, C., Landerer, F. W. (2015). Improved methods for observing Earth's time variable mass distribution with GRACE using spherical cap mascons, J. Geophys. Res. Solid Earth, 120, doi:10.1002/2014JB011547.
Wingham, D. J., et al. (2006), CryoSat: A mission to determine the fluctuations in the Earth's land and marine ice fields, Adv. Space Res., 37,841–871
Wunsch and Stammer (1997). Atmospheric loading and the oceanic "inverted barometer" effect, Rev. Geophys.,35(1), 79–107, doi:10.1029/96RG03037.